Available online at www.sciencedirect.com
ScienceDirect
Physica D 237 (2008) 2777–2786
PHYSICA D
www.elsevier.com/locate/physd

Resonant filtering of compositional waves in multicellular networks

Mete Eray[a,*], Pierre A. Deymier[b], James B. Hoying[c], Keith Runge[d], Jerome O. Vasseur[e]

[a] *Department of Electrical and Computer Engineering, The University of Arizona, Tucson, AZ 85721, United States*
[b] *Materials Science and Engineering Department, The University of Arizona, Tucson, AZ 85721, United States*
[c] *Cardiovascular Innovation Institute, School of Medicine, University of Louisville, Louisville, KY 40292, United States*
[d] *Quantum Theory Project, University of Florida, Gainesville, FL 32611, United States*
[e] *EPHONI, IEMN, UMR CNRS 8520, Université de Lille 1, 59655 Villeneuve d'Ascq, Lille, France*

Received 19 October 2007; received in revised form 17 March 2008; accepted 13 April 2008
Available online 6 May 2008

Communicated by A. Mikhailov

Abstract

Theoretically predicting the stationary and traveling compositional wave patterns observed over trivial multicellular topologies is common place in biology. Systematic methods are needed to find the relationships between the forms of such waves and the underlying network topologies. Here, we introduce one such method based on the Interface Response Theory (IRT) that combines models of intracellular biochemical reactions with those of intercellular networks to analytically track time variations of concentration profiles across nontrivial cellular network topologies. Cellular chains of infinite length are shown to sustain traveling planar waves under certain conditions among the coefficients of the intracellular chemical reactions. A non-trivial cellular network composed of a finite length side chain attached to the infinite backbone leads to the formation of a standing wave pattern upstream from the site of attachment. Downstream, the wave proceeds although a limited number of frequency bands are filtered out of the original content with that number being equal to the number of cells in the side chain.

PACS: 82.20.Wt; 87.22; 82.40.C

Keywords: Biocellular network formation; Interface response theory; Biological pattern formation; Compositional waves

1. Introduction

In recent years, it has become increasingly clear that higher-order biology (e.g. tissue architecture or microenvironment) determines lower-order biology (e.g. genome transcription or enzymatic cascades) and vice versa. Unfortunately, the rules that govern this cross-level interaction and emerging properties associated with this interdependence are poorly understood. Spatio-temporal rhythmic behavior observed in biological systems, ranging from subcellular biochemical molecules to populations of different species, is a direct manifestation of a collective effort to self organize [1]. Identical biochemical content and morphology for the participating entities in such biological systems precludes global control by a single member as the mechanism of coordination. Instead, local molecule-to-molecule [2], organelle-to-organelle [3], cell-to-cell [4,5] or organism-to-organism [6] interactions lead to spatio-temporal pattern formation. In multicellular domains, these interactions can be surprisingly simple such as the *receptor-ligand* binding involved in Delta-Notch signaling pathway [7] or even simpler as in diffusion of inositol (1, 4, 5)-triphosphate (IP_3) and Ca^{2+} participating in intracellular and intercellular Ca^{2+} waves [8]. Despite this simplicity, the emergent behavior can be quite complex such as the three-dimensional, spiraling cAMP waves that accompany the slime mold *Dictyostelium discoideum* morphogenesis [9], glycolytic oscillations observed in yeast, chaotic oscillations during Ca^{2+} signaling [10] and fractal shapes encountered during bacterial colony growth [11] among others. Such interactions are believed to provide certain means for *morphogenesis*, the process of shape formation, perhaps best exemplified by the transformation from the approximately

* Corresponding author.
E-mail address: meray@ece.arizona.edu (M. Eray).

0167-2789/$ - see front matter © 2008 Elsevier B.V. All rights reserved.
doi:10.1016/j.physd.2008.04.020

spherical shape of a few stem cells into the intricate shapes of various organs and organisms [12].

Understanding the cross-level interdependence in multicellular structures means understanding multicellular architectures (high-level organization) and the processes that govern the transmission of information between its constitutive elements (e.g. cells, groups of cells), i.e. the protocols that encodes the cues and regulate the working of the system. The objective of this paper is to introduce the foundations for the development of a new theoretical framework for the integration of lower-order activity (cell function) with higher-order, multicellular architecture to produce a multilevel description of biological organization and function in tissues. From a theoretical point of view, the problem of behavior of a multicellular architecture is that of a network that combines dynamical and structural complexity. The problem at hand is, therefore, to construct a framework for integrating models of intracellular pathways with non-trivial multicellular architectures including cell-to-cell interactions. The signaling pathways could be described by coupled linear or nonlinear, multi-components reactions. The non-trivial multicellular architectures may be one-, two- and three-dimensional with topological complexity (e.g. chains, loops, tubes, sheets, slabs and combinations thereof). Cell-to-cell interactions may include short- and long-range diffusion-driven (involving mass transport) or signal-driven (non-diffusive) coupling. The multicellular architecture may be embedded into extra-cellular media.

In a review article on complex networks, Strogatz proposed some broad generalization concerning the collective behavior of coupled dynamical network nodes [13]. He considers three cases, namely when the nodes of a network are dynamical systems with long-time behavior given by stable fixed points, limit cycles or chaotic attractors. In the case where a node has a stable limit cycle, a structure composed of coupled dynamical nodes may lead to organization in the form of synchronized states such as traveling waves, spatiotemporal chaos and incoherence and mixed-temporal phases of coherent and incoherent states [14–16]. For nodes with stable fixed point the coupled structure may lock into a frustrated glass-like state with multiple local stable equilibria. There is no simple rule for describing coupled architectures of nodes with chaotic behavior but these nodes can also synchronize. Strogatz also remarks that all studies of coupled dynamical systems have been limited to regular network topologies such as chains, grid, lattices or fully connected graphs. The complexity of the collective behavior of these regular structures is completely determined by the nonlinear dynamics of the nodes or of their coupling. The difficulty associated with the combined complexity of the dynamics and architecture has led researchers to take a complementary approach where the dynamics of the nodes is set aside and the emphasis is placed on the complexity of the network architecture [17].

Computer simulations of multicellular systems [18] and tissue have provided useful information concerning the dynamics of pattern formation in reaction-diffusion models of multicellular organism [19], or morphogenesis in embryos [20], or microvascularization and tumor growth [21,22]. However, while computer simulations can account efficiently for very complex dynamics and structures, they lack the generality associated with fundamental underlying principles that can be revealed by simpler models. “Simple” models have been shown to produce far reaching results. In his pioneering mathematical treatise of morphogenesis, Turing demonstrated the possibility of oscillations in a circular chain of cells each carrying the same pair of linearly interacting morphogens [23]. Othmer and Scriven in a fundamental paper tackled the problem of reaction-diffusion in networks of discrete compartment or cells [24]. These authors developed an analysis technique in which the information about the underlying topology, incorporated through a connectivity matrix, is decoupled from that of the linear reaction mechanism. This linear method enables the study of the onset of instability in arbitrary networks. In addition to its relevance to multicellular biological structures, this method has been applied to the study of Turing instabilities in small arrays of diffusively coupled reactors [25]. Othmer and Scriven’s method was extended by Plahte [26,27] to the study of linear stability in diffusion-driven cell-to-cell interactions and signaling-driven models such as the juxtacrine cell-cell signaling model for Delta-Notch lateral inhibition [7]. Plahte argues, though, that linear analysis must be complemented by nonlinear analysis to explain pattern formation. Owen investigated the waves in discrete reaction-diffusion systems where the coupling between sites representing juxtacrine cell signaling is nonlinear [28,29].

Within this general context, we establish the basis for the implementation of a linear theory of multicellular structures that enables the determination of compositional excursions from steady state values in complex multicellular networks. Although we initially focus on advancing a linear theory of complex multicellular architectures, this formalism for reaction-diffusion signaling and Green’s function-based Interface Response Theory (IRT) can enable the development of a nonlinear theory of complex multicellular architectures by providing linear solutions to complex architectures that can be used as starting approximations for perturbative methods.

The work presented here is based on Othmer and Scriven formalism where provided that the system has already reached a steady state point and the eigenvalues and eigenvectors of the connectivity matrix describing the network of interacting cells can explicitly be written, one can obtain a compact, analytical solution for small temporal variations of the reacting/diffusing biochemical species in each cell along the particular topology. In order to apply this method to tackling problems involving non-trivial topologies, we use the Interface Response Theory (IRT) [30]. IRT is a general purpose methodology to find the Green’s function between two arbitrary points in a composite medium in terms of its constitutive parts. This procedure then enables the determination of the eigenvalues and eigenvectors of the composite system in a systematic fashion.

This paper presents a unified method based on Scriven and Othmer’s analysis and IRT. Starting from an infinite length chain of cells as a backbone, the method can be used to build increasingly more complex networks in an algorithmic fashion.

Throughout, it preserves the capability of analytically tracking the small temporal excursions of the constitutive reactants at any location on the multicellular topology. This is demonstrated for the cells constituting the infinite backbone. Filtering of certain spatial frequencies, certainly a nontrivial behavior, emerges as a result of adjoining a finite length segment of cells onto the backbone. In Section 2, an infinite chain of cells carrying linearly interacting reactants is shown to sustain traveling plane waves. A short summary of IRT is presented in Section 3. When a finite length segment is attached to the infinite backbone, the determination of the eigenvalues and the eigenvectors of the composite system using IRT is given in Section 4. An effective transmission coefficient between the right half and the left half of the infinite backbone emerges as a function of wave number is given and the filtering action is explained. In the last section, future work is outlined and potential utility of our method for the analysis of composite multicellular networks is discussed. As such, we are providing an alternative mechanism for generating form via changes in topology [31].

2. Traveling waves across cellular chains

In the half century since Alan Turing's original work [23] on chemical morphogenesis, equation systems of *reaction-diffusion* type and their analytical/numerical solutions have steadily gained importance in the analysis and synthesis of biological systems [24,32]. Turing, assuming each cell carrying the same set of chemical reactants (*morphogens*) X and Y at different concentrations, defined the general system as a set of coupled, ordinary differential equations (ODEs) given by

$$\begin{aligned}\frac{\partial X_r}{\partial t} &= f\,(X_r, Y_r) + D_X \nabla^2 X_r \\ \frac{\partial Y_r}{\partial t} &= g\,(X_r, Y_r) + D_Y \nabla^2 Y_r.\end{aligned} \tag{1}$$

In Eq. (1), X_r and Y_r represent both the reactant and its concentration in cell r. f and g are in general nonlinear and represent the *reaction* part of the equation for X and Y, respectively. The product of the diffusion constant $D_X(D_Y)$ and the Laplacian $\nabla^2 X(\nabla^2 Y)$ forms the *diffusion* part. Assuming small excursions $x_r(y_r)$, $r = 1, \ldots, N$, around quiescent operating points $X_0(Y_0)$, Turing approximated f and g by linear functions of x_r and y_r. For a particular topology, namely a finite ring of N cells, the Laplacian $\nabla^2 X$ was then substituted by its finite difference approximation $x_{r+1} - 2x_r + x_{r-1}$. Known spatial periodicity of the solutions facilitated the representation of the general forms for x_r and y_r as finite sums of complex exponentials similar to Fourier Series decomposition [33]. The resulting set of linear ODEs in terms of a new, decoupled set of variables were then solved using standard ODE techniques and the results were converted back to obtain expressions for x_r and y_r. Turing showed how these solutions could, under certain conditions, approximate both standing and traveling waves.

Othmer and Scriven, while analyzing the onset of instability at homogeneous steady states of multicellular networks, developed an elegant new method that decouples the biochemical *dynamics* from the network *structure* of the underlying *reaction/diffusion* problem [24]. They assumed a mixture of $n \in \mathrm{N}$ reactants in each one of the $N \in \mathrm{N}$ cells, each attached to one or more other cells to form the desired topology. With the small excursions around the steady-state concentration values of cell μ represented by the $n \times 1$ vector $\mathbf{x}^{(\mu)}$, Scriven and Othmer transformed Turing's original formulation given in Eq. (1) into a vector differential equation given by

$$\frac{\mathrm{d}\mathbf{x}^{(\mu)}}{\mathrm{d}t} = \mathbf{D}\Delta^{(\mu)}\mathbf{x}^{(\mu)} + \mathbf{K}\mathbf{x}^{(\mu)}, \quad \mu = 1, \ldots, N. \tag{2}$$

The first term on the right side gives the rates of change due to transfer between directly interacting cells. The rates of change due to intracellular reactions and interactions with the bathing solution are represented by the second part. The element $d_{i,j} \in \mathrm{R}$, $i, j = 1, \ldots, n$, of the $n \times n$ transfer matrix $\mathbf{D}$ quantifies the effect of reactant j on the transfer of reactant i through the barrier separating adjacent cells. The $n \times n$ gradient $\Delta^{(\mu)}\mathbf{x}^{(\mu)}$ in Eq. (2) encodes the connection pattern among the cells and the location index on the gradient operator is dropped whenever each cell has the same connection pattern at any site within the topology. We use $\mathbf{C_x}$ to represent the resulting structural matrix and preserve the notation Δ to be used in the development of IRT. The reaction matrix $\mathbf{K}$ represents the intracellular reaction dynamics and the interaction of the cell's reactants with the external bathing solution with the element $k_{i,j} \in \mathrm{R}$, $i, j = 1, \ldots, n$, representing the collective effect of reactant j on the reactant i. Assuming spatially homogeneous systems, both $\mathbf{D}$ and $\mathbf{K}$ are cell-independent. After several steps of tensor analysis that can be followed from the original manuscript [24], the time progress of concentration excursions in all of the cells are concatenated into an $Nn \times 1$ column vector given by

$$\bar{\mathbf{x}}(t) = \sum_{k=1}^{N} \mathbf{u}_k \otimes \mathrm{e}^{(\mathbf{K}+\alpha_k \mathbf{D})t}\mathbf{y}_k^0 \tag{3}$$

with $\otimes$ representing the tensor product. In Eq. (3), α_k and $\mathbf{u}_k$, $k = 1, \ldots, N$, are the eigenvalues and eigenvectors of $\mathbf{C_x}$, respectively. The $n \times 1$ vector $\mathbf{y}_k^0$ is the projection of the initial condition vector $\bar{\mathbf{x}}_0 = \bar{\mathbf{x}}(t = 0)$ onto a derived set of basis vectors spanning the vector space that includes $\mathbf{x}\,(t)$. In [24], Turing results for a circular chain were successfully reproduced and the conditions for standing and traveling wave formation were discussed. Here, we use Interface Response Theory (IRT) to augment the Scriven–Othmer method in order to solve for the eigenvalues and eigenvectors of an arbitrary connectivity matrix. We demonstrate the technique by providing an analytical representation of concentration excursions in each element of an infinite length cellular chain when a finite length chain is attached at an arbitrary location.

The structural matrix $\mathbf{C}_\infty$ of the infinite chain that forms the backbone in this work (Fig. 1) has the familiar tridiagonal form similar to the circular chain studied in [23,24] as given by

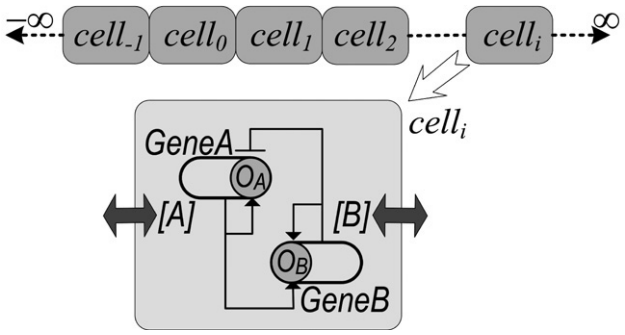

Fig. 1. Infinite chain of cells, each encapsulating a negative feedback circuit.

$$\mathbf{C}_\infty = \begin{pmatrix} \ddots & \ddots & \ddots & \ddots & & & & & & \\ \ddots & \ddots & \ddots & \ddots & \ddots & & & & & \\ \cdots & 0 & 1 & -2 & 1 & 0 & \cdots & & & \\ & \cdots & 0 & 1 & -2 & 1 & 0 & \cdots & & \\ & & \cdots & 0 & 1 & -2 & 1 & 0 & \cdots & \\ & & & \cdots & 0 & 1 & -2 & 1 & 0 & \cdots \\ & & & & & \ddots & \ddots & \ddots & \ddots & \ddots \\ & & & & & & \ddots & \ddots & \ddots & \ddots \end{pmatrix}. \tag{4}$$

The three nonzero entries in each row correspond to the coefficients in the discrete approximation of the Laplacian as in $\nabla^2\mathbf{x}^{(\mu)}(t) = \mathbf{x}^{(\mu+1)}(t) - 2\mathbf{x}^{(\mu)}(t) + \mathbf{x}^{(\mu-1)}(t)$. The corresponding eigenvalues and eigenvectors are given by [34],

$$\begin{aligned} \alpha_k &= -4\sin^2\left(\frac{ka_0}{2}\right) \\ \mathbf{u}_k &= \begin{pmatrix} \cdots & \mathrm{e}^{-\mathrm{i}ka_0} & 1 & \mathrm{e}^{\mathrm{i}ka_0} & \cdots \end{pmatrix}^{\mathrm{T}} \end{aligned} \tag{5}$$

where $k \in \mathrm{Z}$ is the propagation constant and $a_0 \in \mathrm{R} > 0$ is the lattice constant. Notice that each eigenvector is of infinite length and its mth element $u_{k,m}$ represents the mth cell in the chain, where $m \in \mathrm{Z}$. These results are very similar in form to the ones found for finite circular chains [24] and hence hint at the existence of traveling waves across infinite chains as well.

Within each cell, we take $n = 2$ for analytical tractability. We also discard diffusion between the cells and the bathing solution to make $\mathbf{K}$ only a function of the intracellular reaction dynamics. For the sake of mathematical simplicity, we take the active and passive diffusivities to be the same for both reactants such that

$$\mathbf{D} = \begin{pmatrix} d' & d \\ d & d' \end{pmatrix}. \tag{6}$$

For the intracellular dynamics, an *activator/inhibitor* pair is assumed so that

$$\mathbf{K} = \begin{pmatrix} r' & -r \\ r & r' \end{pmatrix}. \tag{7}$$

The constants $d', r' \in \mathrm{R} < 0$ on the main diagonals are self regulation terms whereas the off-diagonal terms d, $r \in \mathrm{R} > 0$ are cross coupling terms. The opposite signs for the off-diagonal elements in $\mathbf{K}$ are sufficient to obtain a self oscillatory behavior for negligible r' [35]. As will be seen shortly, the magnitudes of d' and r' play a role in the attenuation of a traveling plane wave but otherwise do not alter the traveling wave part of the solution presented here.

To demonstrate the sustenance of traveling waves once initiated, initial profiles of spatial exponential variations of wave vector k_0 are assumed for both reactants in cell m. With an arbitrary phase difference of $-\pi \le \theta \le \pi$, the initial condition for cell m is given by

$$\mathbf{x}_0^{(m)} = \begin{pmatrix} \mathrm{e}^{\mathrm{i}k_0a_0m} \\ \mathrm{e}^{\mathrm{i}(k_0a_0m+\theta)} \end{pmatrix}. \tag{8}$$

Such profiles can be thought of as snapshots in time of traveling waves. The following derivation shows that such waves are indeed sustained under certain conditions and otherwise decay exponentially. The projection vector $\mathbf{y}_k^0$ [24] can now be written as,

$$\mathbf{y}_k^0 = \sum_{m=-\infty}^{\infty} u_{k,m}^* \mathbf{x}_0^{(m)} = \begin{pmatrix} \delta_{k,k_0} \\ \delta_{k,k_0}\mathrm{e}^{\mathrm{i}\theta} \end{pmatrix} \tag{9}$$

where δ_{k,k_0} is the Kronecker delta function and is equal to 1 when $k = k_0$ and to 0, otherwise. The notation $(\cdot)^*$ is used for complex conjugation. To write a closed form expression for Eq. (1), the matrix exponential needs to be worked out first. For distinct eigenvalues of the matrix $\mathbf{K} + \alpha_k\mathbf{D}$, Singular Value Decomposition (SVD) method could be used for this task [36]. To search for conditions under which distinctness is satisfied, the eigenvalues are found by solving $|(\mathbf{K} + \alpha_k\mathbf{D} - \lambda\mathrm{I}_2)| = 0$ and are expressed as

$$\begin{aligned} \lambda_k^{(1)} &= \alpha_k d' + r' + \sqrt{\alpha_k^2 d^2 - r^2} \\ \lambda_k^{(2)} &= \alpha_k d' + r' - \sqrt{\alpha_k^2 d^2 - r^2}. \end{aligned} \tag{10}$$

As the structural eigenvalues satisfy $-4 \le \left|\alpha_k^2\right| \le 0$ and thus ensuring that the arguments of the square root terms are negative, Eq. (10) yields a set of complex conjugate eigenvalues and enables the solution of the matrix exponential in Eq. (3) using *SVD*. To do so, the eigenvector equation $(\mathbf{K} + \alpha_k\mathbf{D})\,\boldsymbol{\eta}_k = \lambda\boldsymbol{\eta}_k$ is solved for $\boldsymbol{\eta}_k$ to obtain

$$\boldsymbol{\eta}_k^{(1)} = \begin{pmatrix} \sqrt{\frac{1}{2} + \gamma_k} \\ \sqrt{\frac{1}{2} - \gamma_k} \end{pmatrix}, \qquad \boldsymbol{\eta}_k^{(2)} = \begin{pmatrix} \sqrt{\frac{1}{2} + \gamma_k} \\ -\sqrt{\frac{1}{2} - \gamma_k} \end{pmatrix}, \tag{11}$$

in which the factor $\gamma_k = \frac{r}{2\alpha_k d}$ is a measure of the relative strengths of cross-coupled reaction to cross-coupled diffusion terms. Matrix exponential in Eq. (3) can now be expanded as

$$\mathrm{e}^{(\mathbf{K}+\alpha_k\mathbf{D})t} = \frac{1}{2}\begin{pmatrix} \boldsymbol{\eta}_k^{(1)} & \boldsymbol{\eta}_k^{(2)} \end{pmatrix}\begin{pmatrix} \mathrm{e}^{\lambda_k^{(1)}} & 0 \\ 0 & \mathrm{e}^{\lambda_k^{(2)}} \end{pmatrix}\begin{pmatrix} \boldsymbol{\eta}_k^{(1)} & \boldsymbol{\eta}_k^{(2)} \end{pmatrix}^{\mathrm{T}}. \tag{12}$$

Using Eqs. (10) and (11) in Eq. (12) yields Box I.

$$e^{(\mathbf{K}+\alpha_k\mathbf{D})t} = \frac{1}{2}\begin{pmatrix} e^{\lambda_k^{(1)}} + e^{\lambda_k^{(2)}} & \left(e^{\lambda_k^{(1)}} - e^{\lambda_k^{(2)}}\right)\sqrt{\dfrac{1+2\gamma_k}{1-2\gamma_k}} \\ \left(e^{\lambda_k^{(1)}} - e^{\lambda_k^{(2)}}\right)\sqrt{\dfrac{1+2\gamma_k}{1-2\gamma_k}} & e^{\lambda_k^{(1)}} + e^{\lambda_k^{(2)}} \end{pmatrix} \tag{13}$$

Box I.

$$\mathbf{x}^{(m)}(t) = \frac{1}{2}\begin{pmatrix} e^{ik_0a_0m}\left(e^{\lambda_{k_0}^{(1)}t} + e^{\lambda_{k_0}^{(2)}t}\right) + e^{i(k_0a_0m+\theta)}\left(e^{\lambda_{k_0}^{(1)}t} - e^{\lambda_{k_0}^{(2)}t}\right)\sqrt{\dfrac{1+2\gamma_{k_0}}{1-2\gamma_{k_0}}} \\ e^{ik_0a_0m}\left(e^{\lambda_{k_0}^{(1)}t} - e^{\lambda_{k_0}^{(2)}t}\right)\sqrt{\dfrac{1+2\gamma_{k_0}}{1-2\gamma_{k_0}}} + e^{i(k_0a_0m+\theta)}\left(e^{\lambda_{k_0}^{(1)}t} + e^{\lambda_{k_0}^{(2)}t}\right) \end{pmatrix} \tag{14}$$

Box II.

A closed form general solution for the concentration excursions in cell m is now possible by using Eqs. (5), (9) and (13) in Eq. (3) and is given in Box II.

Neglecting cross-coupling effects in diffusion ($|d| \simeq 0$) leads to $|\gamma_{k_0}| \gg 1$. The square root terms in Eq. (14) can now be simplified as $\sqrt{(1+2\gamma_{k_0})/(1-2\gamma_{k_0})} \simeq \sqrt{-1} = \mathrm{i}$. With this last step, the temporal variations in Eq. (14) of the two concentration excursions within cell m can be expressed as weighted sums of two distinct modes, $e^{\lambda_{k_0}^{(1)}t}$ and $e^{\lambda_{k_0}^{(2)}t}$ as shown below

$$\mathbf{x}^{(m)}(t) \simeq \frac{1}{2}\begin{pmatrix} e^{ik_0a_0m}\left[\left(1+ie^{i\theta}\right)e^{\lambda_{k_0}^{(1)}t} + \left(1-ie^{i\theta}\right)e^{\lambda_{k_0}^{(2)}t}\right] \\ e^{ik_0a_0m}\left[\left(i+e^{i\theta}\right)e^{\lambda_{k_0}^{(1)}t} + \left(e^{i\theta}-i\right)e^{\lambda_{k_0}^{(2)}t}\right] \end{pmatrix}. \tag{15}$$

At $\theta = -\pi/2$, one of the two modes for each reactant is dropped and Eq. (15) is reduced to

$$\mathbf{x}^{(m)}(t) \simeq e^{ik_0a_0m}\begin{pmatrix} e^{\lambda_{k_0}^{(1)}t} \\ -ie^{\lambda_{k_0}^{(2)}t} \end{pmatrix} = e^{ik_0a_0m}\begin{pmatrix} e^{(r'+\alpha_{k_0}d')t}e^{\sqrt{\alpha_{k_0}^2d^2-r^2}t} \\ -ie^{(r'+\alpha_{k_0}d')t}e^{-\sqrt{\alpha_{k_0}^2d^2-r^2}t} \end{pmatrix}. \tag{16}$$

Notice that the two time courses are decoupled as each time profile depends on only one of the two eigenvalues given by Eq. (10). Eq. (16) can be transformed into a more intuitive form by recalling the assumption $|d| \simeq 0$ which in turn validates the assumption $|\alpha_{k_0}d| \ll |r|$. The resulting vector is given by

$$\mathbf{x}^{(m)}(t) = \begin{pmatrix} e^{(r'+\alpha_{k_0}d')t}e^{i(k_0a_0m+rt)} \\ -ie^{(r'+\alpha_{k_0}d')t}e^{i(k_0a_0m-rt)} \end{pmatrix}. \tag{17}$$

The profile for the first component has a backward traveling wave component $e^{i(k_0a_0m+rt)}$ and the second, a forward traveling wave component $e^{i(k_0a_0m-rt)}$. Both profiles also share a common attenuation term $e^{(r'+\alpha_{k_0}d')t}$. The initial $\pi/2$ phase difference is preserved and both waves travel at a constant speed $v = r/k_0$. The leading attenuation term disappears for negligible self promotion/degradation ($r' \simeq 0$) and diffusion ($|d' \simeq 0|$) terms. Otherwise, the traveling wave either reaches a maximum amplitude at which the assumption that lead to Eq. (17) are no longer satisfied or completely disappears depending on the relative magnitudes of r' and d'.

3. Filtering of compositional waves

A multi-dimensional uniform lattice of infinitely many atoms placed at discrete sites has been used as a prototype platform in the development of IRT [37] and is referred to as the *bulk* system. The Green's, or response, function $\mathbf{G}_0$ is the inverse of an operator $\mathbf{H}_0$ that represents the interactions among lattice sites, with element $G_0(n, n')$ denoting the effect observed at site n in response to a perturbation applied at site n'. Inverting $\mathbf{H}_0$ is not trivial for *composite* lattices with nonuniform atoms and/or interactions between atoms as the symmetry in $\mathbf{G}_0$ is lost. The problem becomes more challenging when the lattice deviates into intricate topological shapes, effectively terminating the tridiagonality. IRT was developed to address these issues. Given a base lattice operator $\mathbf{H}_0$ for which the eigenvalues and eigenvectors are analytically available, IRT systematically updates them whenever a certain zone is replaced by a different material, the continuity is lost through a cut or an extra segment of possibly different material is attached [30]. A recent review article [38] and references therein list some of the application areas of IRT with numerous examples from the literature. We address a challenge in biological networks that is isomorphic to the one summarized above.

We use IRT to keep track of the developing eigenvalues and eigenvectors of our cellular network structural matrix as it proceeds to develop from a well-defined initial configuration into a nontrivial final shape. In this work, the initial configuration is the infinite length chain used as a backbone onto which a finite length segment is attached (Fig. 2). We use M to denote the set of sites within the interface domain. In Fig. 2, $cell_0$ and $cell_{1'}$ are the only sites within M.

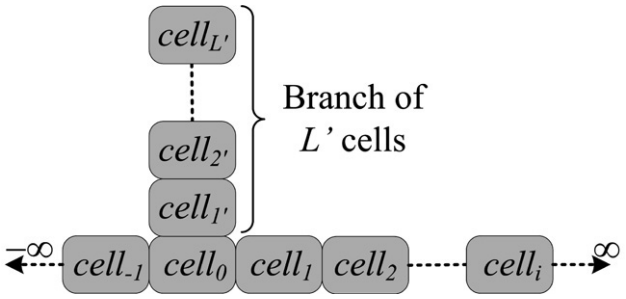

Fig. 2. Composite cellular network formed by coupling a side chain of length L' on an infinite backbone.

The eigenvectors of a composite system depend on those of the bulk system as given by [34]

$$\mathbf{u}(D) = \mathbf{U}(D) - \mathbf{U}(M)^{\mathrm{T}} \boldsymbol{\Delta}^{-1}(M, M)\, \mathbf{A}(M, D), \tag{18}$$

where $\mathbf{U}(D) = \mathrm{e}^{\mathrm{i}ka_0 n}$, $-\infty < n < \infty$, is an eigenvector of the collection of individual bulk systems prior to the coupling operation [34], and $\mathbf{U}(M) = \begin{pmatrix} 1 & 0 \end{pmatrix}^{\mathrm{T}}$ is an eigenvector associated with the interface domain M. $\mathbf{A}(\cdot, \cdot)$ is defined as the interface response operator with the first argument giving the site of the response and the second, the site of the action that leads to the response. The matrix $\boldsymbol{\Delta}(M, M)$ is equivalent to $\mathbf{I}_M + \mathbf{A}(M, M)$ with $\mathbf{I}_M$ being an identity matrix with the dimensions of the set M. The sets D and M limit the spatial extents of the whole composite system and the interface regions, respectively. For our cellular system given in Fig. 2, they are defined as $D = \{D_1 = \{-\infty, \ldots, -1, 0, 1, \ldots, \infty\}\} \cup \{D_2 = \{1', 2', \ldots, L'\}\}$ and $M = \{0, 1'\}$. Notice that M is contained within $D (M \subset D)$. In Eq. (18), $\mathbf{A}(M, D)$ can be written in terms of a coupling operator, $\mathbf{V_I}(M, M)$, applied to the Green's function between points in M and D as given by

$$\mathbf{A}(M, D) = \mathbf{V_I}(M, M)\, \mathbf{G}(M, D). \tag{19}$$

The 2×2 matrix form of $\mathbf{V_I}(M, M)$ is given by,

$$\mathbf{V_I}(M, M) = \begin{pmatrix} -1 & 1 \\ 1 & -1 \end{pmatrix}. \tag{20}$$

In this matrix, the first and second columns or rows correspond to the $cell_0$ of the infinite and $cell_{1'}$ of the side chains, respectively. Notice that $\mathbf{G}(M, D)$ in Eq. (19) is the Green's function of the composite system prior to the attachment of the side chain onto the backbone. Depending on its arguments, $\mathbf{G}(M, D)$ can take one of four possible forms;

$$\mathbf{G}(m \in M, n \in D) = \begin{cases} \mathbf{G_0}(m, n), & \text{if } m = 0 \text{ and } n \in D_1, \\ 0, & \text{if } m = 1' \text{ and } n \in D_1, \\ \mathbf{g_s}(m, n), & \text{if } m = 1 \text{ and } n \in D_2, \\ 0, & \text{if } m = 0 \text{ and } n \in D_2, \end{cases} \tag{21}$$

where $\mathbf{G}_0(\cdot, \cdot)$ is the Green's function of the infinite chain and $\mathbf{g}_s(\cdot, \cdot)$ is that of the side chain. $\mathbf{G}_0(\cdot, \cdot)$ was previously given as [39]

$$\mathbf{G_0}(m, n) = \frac{t^{|m-n|+1}}{t^2 - 1}, \tag{22}$$

where $t = \mathrm{e}^{\mathrm{i}ka_0}$. $\mathbf{g}_s(\cdot, \cdot)$ was derived as [40]

$$\mathbf{g}_s(m, n) = \frac{t^{|m-n|+1} + t^{(m+n)}}{t^2 - 1} + \frac{t^{2L'+1}}{\left(t^2 - 1\right)\left(1 - t^{2L'}\right)} \times \left(t^{(1-m-n)} + t^{(n-m)} + t^{(m-n)} + t^{(m+n-1)}\right). \tag{23}$$

Using the identity given in Eq. (19), components of the interface response operator are listed as

$$\begin{aligned} &\mathbf{A}(0, n) = \mathbf{V_I}(0, 0)\, \mathbf{G}(0, n) \quad \text{for } -\infty < n < \infty, \\ &\mathbf{A}(0, n') = \mathbf{V_I}(0, 1')\, \mathbf{g_s}(1', n') \quad \text{for } 1' < n' < L', \\ &\mathbf{A}(1', n) = \mathbf{V_I}(1', 0)\, \mathbf{G}(0, n) \quad \text{for } -\infty < n < \infty, \\ &\mathbf{A}(1', n') = \mathbf{V_I}(1', 1')\, \mathbf{g_s}(1', n') \quad \text{for } 1' < n' < L'. \end{aligned} \tag{24}$$

The interface response operator between the domains M and D can now be written as a 2×1 matrix as

$$\mathbf{A}(M, D) = \begin{pmatrix} A(0, n) \\ A(1', n) \end{pmatrix} = \begin{pmatrix} V_I(0, 0)\, G_0(0, n) \\ V_I(1', 0)\, G_0(0, n) \end{pmatrix} = \frac{\mathrm{e}^{\mathrm{i}ka_0(1+|n|)}}{\mathrm{e}^{\mathrm{i}2ka_0} - 1} \begin{pmatrix} -1 \\ 1 \end{pmatrix}. \tag{25}$$

Moreover, the inverse of $\boldsymbol{\Delta}(M, M)$ can be derived as in Box III.

Using Eqs. (25) and (26) in Eq. (18), the nth element u_n of the eigenvector $\mathbf{u}_k$ for the composite system is found as

$$u_n = \begin{cases} \mathrm{e}^{\mathrm{i}ka_0 n} + \hat{\Gamma}(\mathrm{i}k)\, \mathrm{e}^{-\mathrm{i}ka_0 n}, & n < 0 \\ \hat{\mathrm{T}}(\mathrm{i}k)\, \mathrm{e}^{\mathrm{i}ka_0 n}, & n \geq 0 \end{cases} \tag{28}$$

where $\hat{\Gamma}(\mathrm{i}k) = \frac{1}{\mathrm{i}2W} \frac{1}{\sin[ka_0]}$ behaves like a reflection coefficient and $\hat{\mathrm{T}}(\mathrm{i}k) = 1 + \hat{\Gamma}(\mathrm{i}k)$ behaves like a transmission coefficient. $\left|\hat{\mathrm{T}}(\mathrm{i}k)\right|^2$ is plotted against ka_0 in Fig. 3. For $0 \leq ka_0 < \pi$, there are exactly L' transmission zeros at which $\left|\hat{\mathrm{T}}(\mathrm{i}k)\right|^2 \simeq 0$. These zeros are located at $z_{ka_0}^{(\nu)} = (\pi/2)(2\nu + 1)/\left(2L' + 1\right)$ for $\nu = 0, 1, \ldots, L'$.

The coupling of a finite length side chain onto the infinite backbone results in the following modified bulk eigenvector

$$\mathbf{u}_k = \begin{pmatrix} \vdots \\ \mathrm{e}^{-i2ka_0} - \left(1 - \hat{\mathrm{T}}(\mathrm{i}k)\right) \mathrm{e}^{\mathrm{i}2ka_0} \\ \mathrm{e}^{-\mathrm{i}ka_0} - \left(1 - \hat{\mathrm{T}}(\mathrm{i}k)\right) \mathrm{e}^{\mathrm{i}ka_0} \\ \hat{\mathrm{T}}(\mathrm{i}k) \\ \mathbf{u}_k\left(1', \ldots, L'\right)^{\mathrm{T}} \\ \hat{\mathrm{T}}(\mathrm{i}k)\, \mathrm{e}^{\mathrm{i}ka_0} \\ \hat{\mathrm{T}}(\mathrm{i}k)\, \mathrm{e}^{\mathrm{i}2ka_0} \\ \vdots \end{pmatrix}_{\infty \times 1}, \tag{29}$$

where $\mathbf{u}_k\left(1', \ldots, L'\right)^{\mathrm{T}}$ is a column vector representing the elements of the finite side chain eigenvectors. Notice that

$$\boldsymbol{\Delta}^{-1}(M,M) = \left(\mathbf{I}_M + \begin{pmatrix} A(0,0) & A(0,1') \\ A(1',0) & A(1',1') \end{pmatrix}\right)^{-1}$$
$$= \frac{1}{W}\begin{pmatrix} 1 - \frac{1}{2}\frac{\cos\left[\left(L'-1/2\right)ka_0\right]}{\sin\left[ka_0/2\right]\sin\left[ka_0L'\right]} & -\frac{1}{2}\frac{\cos\left[\left(L'-1/2\right)ka_0\right]}{\sin\left[ka_0/2\right]\sin\left[ka_0L'\right]} \\ \frac{1}{2}\frac{\mathrm{i}}{\sin\left[ka_0\right]} & 1+\mathrm{i}\frac{1}{2}\frac{1}{\sin\left[ka_0\right]} \end{pmatrix} \tag{26}$$

with

$$W = 1 + \frac{\mathrm{i}}{2\sin\left[ka_0\right]} - \frac{1}{2}\frac{\cos\left[\left(L'-1/2\right)ka_0\right]}{\sin\left[ka_0/2\right]\sin\left[ka_0L'\right]} \tag{27}$$

Box III.

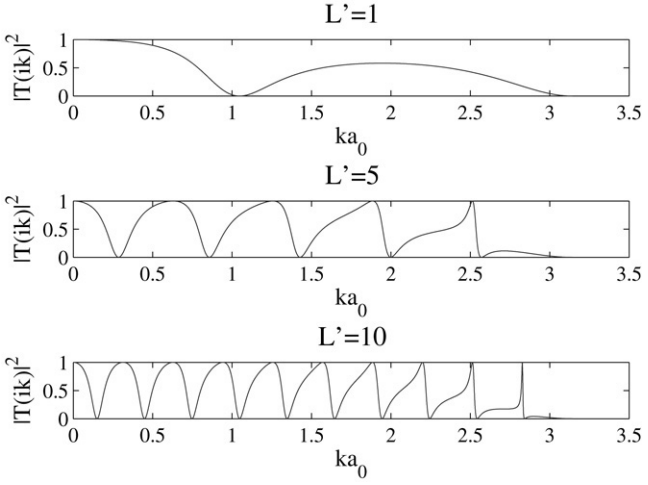

Fig. 3. Transmission spectrum along the infinite chain coupled to a side chain of length $L' = 1, 5, 10$.

the addition of the side branch leads to the breaking of the symmetry of the eigenvectors relative to those of the infinite backbone given by Eq. (5). Since our focus in this work is on the compositional wave propagation and filtering along the infinite backbone, the details of $\mathbf{u}_k\left(1',\ldots,L'\right)^{\mathrm{T}}$ are nonconsequential and are thus delegated to a future work. The eigenvector in Eq. (29) can be decomposed into three independent parts, $\mathbf{u}_k = \mathbf{u}_k^{(1)} + \mathbf{u}_k^{(2)} + \mathbf{u}_k^{(3)}$, and the nth components of each one of these are given by

$$u_{k,n}^{(1)} = \left\{\begin{matrix} \mathrm{e}^{\mathrm{i}nka_0} - (1-\hat{\mathrm{T}}(\mathrm{i}k))\mathrm{e}^{-\mathrm{i}nka_0}, & \text{for } n \le 0 \\ 0, & \text{elsewhere} \end{matrix}\right\},$$
$$u_{k,n}^{(2)} = \left\{\begin{matrix} u_k(n), & \text{for } 1 \le n \le L' \\ 0, & \text{elsewhere} \end{matrix}\right\}, \tag{30}$$
$$u_{k,n}^{(3)} = \left\{\begin{matrix} \hat{\mathrm{T}}(\mathrm{i}k)\mathrm{e}^{\mathrm{i}nka_0}, & \text{for } L'+1 \le n \\ 0, & \text{elsewhere} \end{matrix}\right\},$$

We further decomposed $\mathbf{u}_k^{(1)}$ into three parts, $\mathbf{u}_k^{(1)} = \mathbf{u}_k^{(1)(1)} + \mathbf{u}_k^{(1)(2)} + \mathbf{u}_k^{(1)(3)}$ with each subcomponent defined as

$$u_{k,n}^{(1)(1)} = \left\{\begin{matrix} \mathrm{e}^{\mathrm{i}nka_0}, & \text{for } n \le -1 \\ 0, & \text{elsewhere} \end{matrix}\right\},$$
$$u_{k,n}^{(1)(2)} = \left\{\begin{matrix} -\mathrm{e}^{-\mathrm{i}nka_0}, & \text{for } n \le -1 \\ 0, & \text{elsewhere} \end{matrix}\right\}, \tag{31}$$
$$u_{k,n}^{(1)(3)} = \left\{\begin{matrix} \hat{\mathrm{T}}(\mathrm{i}k)\mathrm{e}^{-\mathrm{i}nka_0}, & \text{for } n \le 0 \\ 0, & \text{elsewhere} \end{matrix}\right\}.$$

Next, we define the initial conditions for the concentration excursions around steady state values for the cells in the backbone as before. For the cells in the side chain, we assume zero initial conditions. The initial condition vector given by Eq. (8) for the infinite backbone is now modified for the composite system as given by

$$\mathbf{x}_0^{(m)} = \begin{cases} \begin{pmatrix} \mathrm{e}^{\mathrm{i}k_0a_0m} \\ \mathrm{e}^{\mathrm{i}k_0a_0m}\mathrm{e}^{\mathrm{i}\theta} \end{pmatrix}, & \text{for } m \le 0 \\ \begin{pmatrix} 0 \\ 0 \end{pmatrix}, & \text{for } 1 \le m \le L' \\ \begin{pmatrix} \mathrm{e}^{\mathrm{i}k_0a_0m} \\ \mathrm{e}^{\mathrm{i}k_0a_0m}\mathrm{e}^{\mathrm{i}\theta} \end{pmatrix}, & \text{for } m > L'. \end{cases} \tag{32}$$

Notice that the initial conditions corresponding to the finite side chain are inserted within the form given by Eq. (8), effectively breaking the symmetry around $m = 0$. The projection vector $\mathbf{y}_k^0$ given in Eq. (9) can now be constructed as a weighted superposition of initial cellular concentration excursions as

$$\begin{aligned} \mathbf{y}_k^0 &= \sum_{m=-\infty}^{\infty} u_{k,m}^{*}\mathbf{x}_0^{(m)} \\ &= \sum_{m=-\infty}^{0} u_{k,m}^{(1)*}\mathbf{x}_0^{(m)} + \sum_{m=1}^{L'} u_{k,m}^{(2)*}\mathbf{x}_0^{(m)} + \sum_{m=L'+1}^{\infty} u_{k,m}^{(3)*}\mathbf{x}_0^{(m)} \\ &= \sum_{m=-\infty}^{-1} u_{k,m}^{(1)(1)*}\mathbf{x}_0^{(m)} + \sum_{m=-\infty}^{-1} u_{k,m}^{(1)(2)*}\mathbf{x}_0^{(m)} \\ &\quad + \sum_{m=-\infty}^{0} u_{k,m}^{(1)(3)*}\mathbf{x}_0^{(m)} + \sum_{m=L'+1}^{\infty} u_{k,m}^{(3)*}\mathbf{x}_0^{(m)}. \end{aligned} \tag{33}$$

The first semi-infinite series can be simplified as

$$\begin{aligned} \sum_{m=-\infty}^{-1} u_{k,m}^{(1)(1)} * \mathbf{x}_0^{(m)} &= \sum_{m=-\infty}^{-1} \mathrm{e}^{-\mathrm{i}ka_0m}\begin{pmatrix} \mathrm{e}^{\mathrm{i}k_0a_0m} \\ \mathrm{e}^{\mathrm{i}\theta}\mathrm{e}^{\mathrm{i}k_0a_0m} \end{pmatrix} \\ &= \sum_{m=1}^{\infty}\begin{pmatrix} \mathrm{e}^{\mathrm{i}(k-k_0)a_0m} \\ \mathrm{e}^{\mathrm{i}\theta}\mathrm{e}^{\mathrm{i}(k-k_0)a_0m} \end{pmatrix} \\ &= \begin{pmatrix} 1 \\ \mathrm{e}^{\mathrm{i}\theta} \end{pmatrix}\left\{\mathrm{I}(k_0,k) - 1\right\}, \end{aligned} \tag{34}$$

$$\mathbf{x}^{(m)}(t) \simeq \mathrm{e}^{(r'+\alpha_{k_0}d')t}\begin{pmatrix} \hat{\mathrm{T}}(\mathrm{i}k_0)^*\,\mathrm{e}^{\mathrm{i}(rt-k_0a_0m)} - \left(1-\hat{\mathrm{T}}(\mathrm{i}k_0)\right)\hat{\mathrm{T}}(\mathrm{i}k_0)^*\,\mathrm{e}^{\mathrm{i}(rt+k_0a_0m)} \\ -\mathrm{i}\hat{\mathrm{T}}(\mathrm{i}k_0)^*\,\mathrm{e}^{-\mathrm{i}(rt+k_0a_0m)} + \mathrm{i}\left(1-\hat{\mathrm{T}}(\mathrm{i}k_0)\right)\hat{\mathrm{T}}(\mathrm{i}k_0)^*\,\mathrm{e}^{-\mathrm{i}(rt-k_0a_0m)} \end{pmatrix}$$
$$\simeq \mathrm{e}^{(r'+\alpha_{k_0}d')t}\begin{pmatrix} -2\mathrm{i}\hat{\mathrm{T}}(\mathrm{i}k_0)^*\,\mathrm{e}^{\mathrm{i}rt}\sin(k_0a_0m) + \left|\hat{\mathrm{T}}(\mathrm{i}k_0)\right|^2\mathrm{e}^{\mathrm{i}rt}\mathrm{e}^{\mathrm{i}k_0a_0m} \\ -2\hat{\mathrm{T}}(\mathrm{i}k_0)^*\,\mathrm{e}^{-\mathrm{i}rt}\sin(k_0a_0m) - \mathrm{i}\left|\hat{\mathrm{T}}(\mathrm{i}k_0)\right|^2\mathrm{e}^{-\mathrm{i}rt}\mathrm{e}^{\mathrm{i}k_0a_0m} \end{pmatrix} \tag{43}$$

Box IV.

where

$$\mathrm{I}(k_1,k_2) = \sum_{n=0}^{\infty}\mathrm{e}^{-i(k_1-k_2)a_0n} = \frac{\mathrm{e}^{\mathrm{i}a_0(k_1-k_2)}}{-1+\mathrm{e}^{\mathrm{i}a_0(k_1-k_2)}}. \tag{35}$$

Similarly,

$$\begin{aligned} \sum_{m=-\infty}^{-1} u_{k,m}^{(1)(2)*}\mathbf{x}_0^{(m)} &= \begin{pmatrix}1\\ \mathrm{e}^{\mathrm{i}\theta}\end{pmatrix}\{\mathrm{I}(-k,-k_0)-1\} \\ \sum_{m=-\infty}^{0} u_{k,m}^{(1)(3)*}\mathbf{x}_0^{(m)} &= \hat{\mathrm{T}}(\mathrm{i}k)^*\begin{pmatrix}1\\ \mathrm{e}^{\mathrm{i}\theta}\end{pmatrix}\mathrm{I}(-k,-k_0) \end{aligned} \tag{36}$$

and

$$\sum_{m=-\infty}^{0} u_{k,m}^{(3)*}\mathbf{x}_0^{(m)} = \hat{\mathrm{T}}(\mathrm{i}k)^*\begin{pmatrix}1\\ \mathrm{e}^{\mathrm{i}\theta}\end{pmatrix}\{\mathrm{I}(k,k_0)-1\}. \tag{37}$$

Substituting Eqs. (34)–(37) in Eq. (33) leads to the following compact form for $\mathbf{y}_k^0$,

$$\mathbf{y}_k^0 = \begin{pmatrix}1\\ \mathrm{e}^{\mathrm{i}\theta}\end{pmatrix}\{\mathrm{I}(k_0,k) - \mathrm{I}(-k,-k_0) + \mathrm{Z}(k,k_0)\}. \tag{38}$$

The first two terms in the curly bracket cancel each other and the third term is equivalent to

$$\begin{aligned} \mathrm{Z}(k,k_0) &= \mathrm{I}(-k,-k_0) + \mathrm{I}(k,k_0) - 1 \\ &= \frac{2-\mathrm{e}^{\mathrm{i}a_0(k-k_0)}-\mathrm{e}^{\mathrm{i}a_0(-k+k_0)}}{2-\mathrm{e}^{\mathrm{i}a_0(k-k_0)}-\mathrm{e}^{\mathrm{i}a_0(-k+k_0)}} - 1 \\ &= \begin{Bmatrix}0, & \text{if } k=k_0\\ 1, & \text{if } k\neq k_0\end{Bmatrix} \\ &= \delta_{k,k_0}. \end{aligned} \tag{39}$$

Thus,

$$\mathbf{y}_k^0 = \begin{pmatrix}1\\ \mathrm{e}^{\mathrm{i}\theta}\end{pmatrix}\hat{\mathrm{T}}(\mathrm{i}k)^*\,\delta_{k,k_0}. \tag{40}$$

When compared with the projection vector with no side chain present, one notices that the projection vector is modified by the weighing function $\hat{\mathrm{T}}(\mathrm{i}k)^*$. Using this last expression for $\mathbf{y}_k^0$ in Eq. (3) and following the same set of mathematical reasoning used in Section 2, the vector for concentration excursions is given as

$$\mathbf{x}^{(m)}(t) = \sum_{k=-\infty}^{\infty}\hat{\mathrm{T}}(\mathrm{i}k)\,\mathrm{e}^{\mathrm{i}ka_0m}\frac{\hat{\mathrm{T}}(\mathrm{i}k)^*}{2}\delta_{k,k_0}$$
$$\times\begin{pmatrix}\left(\mathrm{e}^{\lambda_k^{(1)}t}+\mathrm{e}^{\lambda_k^{(2)}t}\right)+\mathrm{e}^{\mathrm{i}\theta}\left(\mathrm{e}^{\lambda_k^{(1)}t}-\mathrm{e}^{\lambda_k^{(2)}t}\right)\sqrt{\dfrac{1+2\gamma_k}{1-2\gamma_k}} \\ \left(\mathrm{e}^{\lambda_k^{(1)}t}-\mathrm{e}^{\lambda_k^{(2)}t}\right)\sqrt{\dfrac{1+2\gamma_k}{1-2\gamma_k}}+\mathrm{e}^{\mathrm{i}\theta}\left(\mathrm{e}^{\lambda_k^{(1)}t}+\mathrm{e}^{\lambda_k^{(2)}t}\right)\end{pmatrix} \tag{41}$$

for $m \geq L'+1$, which is the region to the right of the infinite backbone. Using the same set of assumptions that led to the attenuated traveling wave approximation in Section 2, $\mathbf{x}^{(m)}(t)$, $m \geq L'+1$, for the coupled system can be approximated as

$$\mathbf{x}^{(m)}(t) \simeq \left|\hat{\mathrm{T}}(\mathrm{i}k_0)\right|^2\begin{pmatrix}\mathrm{e}^{(r'+\alpha_{k_0}d')t}\mathrm{e}^{\mathrm{i}(rt+k_0a_0m)} \\ -\mathrm{i}\mathrm{e}^{(r'+\alpha_{k_0}d')t}\mathrm{e}^{\mathrm{i}(-rt+k_0a_0m)}\end{pmatrix}. \tag{42}$$

These are still attenuated traveling plane waves as in Eq. (17) for the infinite backbone, however they are now weighted by the function $\left|\hat{\mathrm{T}}(\mathrm{i}k_0)\right|^2$. The wave numbers coinciding with the transmission zeros shown in Fig. 3 are dropped from the original plane wave. To find the solution to the left of the coupled branch, the expression for the elements of the modified eigenvector with $m \leq 0$, $u_{k,m} = \mathrm{e}^{-\mathrm{i}ka_0m} - \left(1-\hat{\mathrm{T}}(\mathrm{i}k)\right)\mathrm{e}^{\mathrm{i}ka_0m}$, replaces $u_{k,m} = \hat{\mathrm{T}}(\mathrm{i}k)\,\mathrm{e}^{\mathrm{i}ka_0m}$ in Eq. (41). The result is in Box IV.

The leading time function in Eq. (43) is the attenuation term similar to those in Eqs. (17) and (42). Eq. (43) reveals a quasi-standing wave nature to the left of the side branch ($m \leq 0$). The first part in each row represents a proper standing wave weighted by $\hat{\mathrm{T}}(\mathrm{i}k)^*$ [41]. The remaining terms in both rows represent traveling waves weighted by $\hat{\mathrm{T}}(\mathrm{i}k)^*$. At the transmission zeros of $\left|\hat{\mathrm{T}}(\mathrm{i}k_0)\right|^2$ (see Fig. 3), the traveling wave components are eliminated, leaving behind a proper standing wave pattern for each reactant weighted by $\hat{\mathrm{T}}(\mathrm{i}k)^*$, a nonzero complex number in general.

The procedure that resulted in Eq. (43) can be used to attach an arbitrary structure with known Green's function at a single cell of the backbone. The general form of the solution given in (43) will be preserved with only $\hat{\mathrm{T}}(\mathrm{i}k_0)$ updated in accordance with the attached structure. In other words, $\hat{\mathrm{T}}(\mathrm{i}k_0)$ carries a signature associated with the topology of the attached structure.

4. Discussion

Theoretical means for forming oscillatory standing and traveling wave patterns over various biocellular network topologies have been successfully demonstrated before [3,4,7,8,10,42,43]. We presented a unified methodology to build

biocellular networks of increasing complexity in a systematic fashion. We first assumed a hypothetical topology of an infinitely long chain of interconnected cells, each encapsulating the same set of reactants interacting in an *activation–inhibition* fashion. For a particular initial phase difference between the two reactants, the chosen topology theoretically sustains this phase difference and exhibits traveling waves. This is provided that attenuation functions that scale the traveling wave components are weak within the time frames of interest. A standing wave pattern formed upstream from the site of attachment when a side branch was coupled onto the infinite length backbone, providing an alternative route to periodic pattern formation that is routinely observed in biological systems [44].

From a biological stand point, these results imply that the breaking of the symmetry in the propagation of compositional waves in the backbone, through the transmission coefficient, imposed by even one side chain (even composed of one single cell) may lead, provided that the cell response goes beyond linearity, to the conversion of the standing wave pattern into tissue heterogeneities such as striping, or in the field of development, to cell division resulting in the budding of additional side branches (i.e. growth of a periodic architecture). The specificity of the signal associated with the architecture may provide a mechanism for structural reinforcement via feedback processes as well as robustness in the development of multicellular architectures, including stabilization with respect to abnormal growth. This work is relevant to 1D architectures constituted of networks of infinite chains of cells, finite chains of cells, loops, etc. These architectures are reminiscent of filamentous cyanobacteria that grow as chain-like multicellular organisms. These organisms exhibit regular patterns of nitrogen fixing heterocyst that serve as models of pattern formation in higher organisms [45,46]. Other types of chain-like cell structures to which our work is relevant, includes networks of human embryonic stem-cells [47]. These 1D architectures will also have applicability in higher level biological organization such as community and ecosystems within the context of multi-patch or metapopulation models [48,49].

The method introduced here may constitute the foundation for the development of a nonlinear theory of complex multicellular architectures. This nonlinear theory may be enabled by the convergence of several areas. The first area is the development of the linear theory of complex multicellular architectures, presented here, that provides linear solutions to complex architectures that can be used as starting approximations for perturbative methods. For instance, in another study of non-biological systems, we have shown that the IRT can be used to generate linear solutions of Euler equation that were subsequently used in conjunction with Nyborg's second-order perturbation formalism to solve the nonlinear Navier-Stokes equation in heterogeneous media [50,51]. The second area is the development of hybrid systems such as piecewise-linear models that possess the essential features of many nonlinear dynamical systems, as for instance, regulatory systems [52,53]. The third area relates to perturbative approaches such as He's Homotopy Perturbation Method (HPM) [54], where a nonlinear operator is separated into its linear and nonlinear parts. An embedding parameter that can vary between 0 and 1 is used to construct an operator that can transition between the linear operator and the original nonlinear one. The solution to the switching operator is assumed to be expandable into a power series of the embedding parameters. Upon taking the limit of the embedding parameter toward 1 one obtains an approximate solution to the original nonlinear operator. The HPM has been shown to be able to effectively solve strongly nonlinear problems including nonlinear parabolic differential equations [55]. The final area is the use of Green's function propagator theory for time dependent processes that enables us to write the Green's function of a perturbed system in terms of a series of integral terms involving the product of Green's function of the unperturbed system and of a perturbation operator [56,57]. The work presented here is therefore a important first step in the development of a nonlinear theory of multicellular architectures.

Acknowledgements

We acknowledge the financial support from the College of Engineering, University of Arizona. P.A.D. acknowledges useful discussions with L. Dobrzynski and B. Djafari-Rouhani.

References

[1] S. Camazine, J. Deneubourg, N.R. Franks, J. Sneyd, G. Theraulaz, E. Bonabeau, Self-Organization in Biological Systems, 1st ed., Princeton University Press, Princeton, 2001.
[2] A.S. Mikhailov, B. Hess, Self-organization in living cells: Networks of protein machines and nonequilibrium soft matter, J. Biol. Phys. 28 (2002) 655–672.
[3] M.H.P. Wussling, K. Krannich, G. Landgraf, A. Herrmann-Frank, D. Wiedenmann, F.N. Gellerich, et al., Sarcoplasmic reticulum vesicles embedded in agarose gel exhibit propagating calcium waves, FEBS Lett. 463 (1999) 103–109.
[4] B. Hess, Periodic patterns in biochemical reactions, Q. Rev. Biophys. 30 (1997) 121–176.
[5] Y. Tang, H.E. Othmer, Excitation, oscillations and wave propagation in a g-protein-based model of signal transduction in dictyostelium discoideum, Phil. Trans. R. Soc. B. 349 (1995) 179–195.
[6] D. Dormann, B. Vasiev, C.J. Weijer, Becoming multicellular by aggregation; The morphogenesis of the social amoebae dicyostelium discoideum, J. Biol. Phys. 28 (2002) 765–780.
[7] J.R. Collier, N.A.M. Monk, P.K. Maini, J.H. Lewis, Pattern formation by lateral inhibition with feedback: A mathematical model of Delta-Notch intercellular signalling, J. Theor. Biol. 183 (1996) 429–446.
[8] J. Sneyd, J. Keizer, M.J. Sanderson, Mechanisms of calcium oscillations and waves: A quantitative analysis, FASEB J. 9 (1995) 1463–1472.
[9] O. Steinbock, F. Siegert, S. Muller, C. Weijer, Three-dimensional waves of excitation during dictyostelium morphogenesis, PNAS 90 (1993) 7332–7335.
[10] A. Goldbeter, Biochemical Oscillations and Cellular Rhythms, Cambridge University Press, Cambridge, 1996.
[11] E. Ben-Jacob, I. Cohen, H. Levine, Cooperative self-organization of microorganisms, Adv. Phys. 49 (2000) 395–554.
[12] L. Wolpert, R. Beddington, J. Brockes, T. Jessell, P. Lawrence, E. Meyerowitz, Principles of Development, 1st ed., Oxford University Press, Oxford, 1998.
[13] S.H. Strogatz, Exploring complex networks, Nature 410 (2001) 268–276.

[14] A.T. Winfree, Biological rhythms and the behavior of populations of coupled oscillators, J. Theor. Biol. 16 (1967) 15–42.
[15] Y. Kuramoto, D. Battogtokh, Coexistence of coherence and incoherence in nonlocally coupled phase oscillators, Nonlin. Phenom. Compl. Syst. 5 (2002) 380–385.
[16] D.M. Abrams, S.H. Strogatz, Chimera states in a ring of nonlocally coupled oscillators, Int. J. Bifurcation Chaos Appl. Sci. Eng. 16 (2006) 21.
[17] D.J. Watts, S.H. Strogatz, Collective dynamics of /'small-world/' networks, Nature 393 (1998) 440–442.
[18] R.L. Schiek, E.E. May, Development of a massively-parallel, biological circuit simulator, Bioinformatics Conference, 2003. CSB 2003. Proceedings of the 2003 IEEE. (11–14 Aug. 2003) 620–622.
[19] D.A. Kessler, H. Levine, Pattern formation in Dictyostelium via the dynamics of cooperative biological entities, Phys. Rev. E. 48 (1993) 4801–4804.
[20] D. Longo, S.M. Peirce, T.C. Skalak, L. Davidson, M. Marsden, B. Dzamba, et al., Multicellular computer simulation of morphogenesis: Blastocoel roof thinning and matrix assembly in Xenopus laevis, Dev. Biol. 271 (2004) 210–222.
[21] V. Cristini, H.B. Frieboes, R. Gatenby, S. Caserta, M. Ferrari, J. Sinek, Morphologic instability and cancer invasion, Clin. Cancer Res. 11 (2005) 6772–6779.
[22] H.B. Frieboes, J.S. Lowengrub, S. Wise, X. Zheng, P. Macklin, E.L. Bearer, et al., Computer simulation of glioma growth and morphology, Neuroimage 37 (2007) S59–S70.
[23] A.E.R. Turing, The chemical basis of morphogenesis, philosophical transactions of the royal society of London. Series B, Biol. Sci. 237 (1952) 1934–1990. 37–72.
[24] H.G. Othmer, L.E. Scriven, Instability and dynamic pattern in cellular networks, J. Theor. Biol. 32 (1971) 507–537.
[25] P.K. Moore, W. Horsthemke, Localized patterns in homogeneous networks of diffusively coupled reactors, Physica D. 206 (2005) 121–144.
[26] E. Plahte, Pattern formation in discrete cell lattices, J. Math. Biol. 43 (2001) 411–445.
[27] E. Plahte, L. Oyehaug, Pattern-generating travelling waves in a discrete multicellular system with lateral inhibition, Physica D., 226, 117–128.
[28] M.R. Owen, Waves and propagation failure in discrete space models with nonlinear coupling and feedback, Physica D. 173 (2002) 59–76.
[29] S.D. Webb, M.R. Owen, Oscillations and patterns in spatially discrete models for developmental intercellular signalling. (Author abstract), J. Math. Biol. 48 (2004) 444(33).
[30] L. Dobrzynski, Interface response theory of discrete composite systems, Surf. Sci. Rep. 6 (1986) 119–157.
[31] S. Miyashita, S. Murata E.R., in: M. Capcarre (Ed.), Topology Changes Enable Reaction-Diffusion to Generate Forms, Springer Verlag, Heidelberg, 2005, pp. 159–168.
[32] S. Kondo, R. Asai, A reaction–diffusion wave on the skin of the marine angelfish Pomacanthus, Nature 376 (1995) 765–768.
[33] A.V. Oppenheim, A.S. Willsky, I.T. Young, Signals and Systems, First ed., Prentice-Hall, Englewood Cliffs, New Jersey, 1983.
[34] L. Dobrzynski, H. Puszkarski, Eigenvectors of composite systems. I. General theory, J. Phys. Condens. Matter. 1 (1989) 1239–1245.
[35] R. Thomas, M. Kaufman, Multistationarity, the basis of cell differentiation and memory. I. Structural conditions of multistationarity and other nontrivial behavior, Chaos 11 (2001) 170–179.
[36] C. Chen, Linear System Theory and Design, 2nd ed., HRW, New York, 1984.
[37] A. Akjouj, B. Sylla, P. Zielinski, L. Dobrzynski, Lattice dynamics of systems with two interfaces, J. Phys. C Solid State Phys. 20 (1987) 6137–6147.
[38] J.O. Vasseur, A. Akjouj, L. Dobrzynski, B. Djafari-Rouhani, E.H. El Boudouti, Photon, electron, magnon, phonon and plasmon mono-mode circuits, Surf. Sci. Rep. 54 (2004) 1–156.
[39] B. Sylla, L. Dobrzynski, H. Puszkarski, Eigenvectors of composite systems. II. Phonon eigenvectors in some layered materials, J. Phys. Condens. Matter. 1 (1989) 1247–1252.
[40] A. Akjouj, B. Sylla, L. Dobrzynski, Introduction à la théorie des systèmes composites: exemples simples de matériaux lamellaires, Annales de Physique 18 (1993) 363–448.
[41] G. Gonzalez, Microwave Transistor Amplifiers, 2nd ed., Prentice Hall, Upper Saddle River, NJ, 1997.
[42] J.D. Murray, Mathematical Biology II: Spatial Models and Biomedical Applications, 3rd ed., Springer Verlag, New York, 2002.
[43] J.P. Keener, Propagation of waves in an excitable medium with discrete release sites, SIAM J. Appl. Math. 61 (2000) 317–334.
[44] J.D. Murray, Mathematical Biology I: An Introduction, 3rd ed., Springer Verlag, New York, 2002.
[45] T.A. Black, Y. Cai, C.P. Wolk, Spatial expression and autoregulation of hetR, a gene involved in the control of heterocyst development in Anabaena, Mol. Microbiol. 9 (1993) 77–84.
[46] H. Yoon, J.W. Golden, Heterocyst pattern formation controlled by a diffusible peptide, Science 282 (1998) 935–938.
[47] N.L. Boyd, S.K. Dhara, R. Rekaya, E.A. Godbey, K. Hasneen, R.R. Rao, et al., BMP4 promotes formation of primitive vascular networks in human embryonic stem cell-derived embryoid bodies, Exp. Biol. Med. 232 (2007) 833–843.
[48] A.L. Lloyd, V.A.A. Jansen, Spatiotemporal dynamics of epidemics: Synchrony in metapopulation models, Math. Biosci. 188 (2004) 1–16.
[49] V.A.A. Jansen, A.L. Lloyd, Local stability analysis of spatially homogeneous solutions of multi-patch systems, J. Math. Biol. 41 (2000) 232–252.
[50] P.A. Deymier, J.O. Vasseur, A. Khelif, S. Raghavan, Second-order sound field during megasonic cleaning of patterned silicon wafers: Application to ridges and trenches, J. Appl. Phys. 90 (2001) 4211–4218.
[51] P.A. Deymier, J.O. Vasseur, A. Khelif, B. DjafariRouhani, L. Dobrzynski, S. Raghavan, Streaming and removal forces due to second-order sound field during megasonic cleaning of silicon wafers, J. Appl. Phys. 88 (2000) 6821–6835.
[52] H. Oktem, A survey on piecewise-linear models of regulatory dynamical systems, Nonlinear Anal. 63 (2005) 336–349.
[53] H. Hardin, J. van Schuppen, System reduction of nonlinear positive systems by linearization and truncation, Positive Syst. (2006) 431–438.
[54] J. He, Some asymptotic methods for strongly nonlinear equations, Int. J. Mod. Phys. B: Condens. Matter Phys.; Stat. Phys.; Appl. Phys. 20 (2006) 1141.
[55] F. Shakeri, M. Dehghan, Inverse problem of diffusion equation by He's homotopy perturbation method, Phys. Scripta. 75 (2007) 551–556.
[56] R.D. Mattuck, A guide to Feynman Diagrams in the many-body problem, McGraw-Hill, New York, 1992.
[57] P. Ramond, Field Theory: A Modern Primer, Benjamin/Cummings, Menlo Park, CA, 1981.